Bulletin du Service Géologique National
Vol. 17, n° 2, pp. 161 - 181, 15 fig., 10 tabl., 2006

SONIC LOG ANALYSIS WITH THE CONTINUOUS WAVELET TRANSFORM

N. ZAOURAR*, L. BRIQUEU**, S. GACI*, M. HAMOUDI* and D. GIBERT***

ABSTRACT

We use the Continuous Wavelet Transform (CWT) to identify lithologic units, notably in terms of discontinuity, based on the analysis of stochastic fluctuations of sonic logs. The use of the CWT seems to be a particularly well adapted tool to extract systematically and reliably the information related to the singular part of the signal. The method has been tested on synthetic models and actual data set obtained from sonic logs in oil exploration. Starting from synthetic fractal models, we show the influence of the various statistical parameters, in particular the number of Hurst which indicates the local regularity of the medium. Its application to real sonic logs confirms the previous results. Indeed, the exponent parameter can be used to identify the transitions of the lithologic units observed in the well. This important result allows to precisely locate the areas of lithologic discontinuity related to lithological variations.

Key words - Scale - Stochastic - Wavelet analysis - Well logs - Discontinuities - Lithologic.

ANALYSE DES DIAGRAPHIES SONIQUES PAR TRANSFORMÉE EN ONDELETTES CONTINUE

RÉSUMÉ

L'étude des variations stochastiques portées par les fluctuations de vitesse des diagraphies soniques permet de caractériser les transitions lithologiques. Nous proposons un algorithme d'analyse des signaux stochastiques qui tire partie de deux techniques puissantes de détection : une analyse locale par Transformée en Ondelettes Continue combinée à l'utilisation des propriétés multiéchelles des signaux. La méthode est développée à partir de modèles synthétiques puis appliquée à des données de diagraphies soniques. Sur les modèles synthétiques, nous montrons l'influence des différents paramètres statistiques, notamment le nombre de Hurst qui traduit la régularité locale du milieu. L'application de la méthode aux données réelles de diagraphie sonique confirme les résultats précédents. Les variations les plus fines sont ainsi détectées et localisées par l'estimation d'un exposant spectral ou de rugosité qui reflète point par point le degré d'hétérogénéité des différentes unités géologiques traversées par un forage.

Mots clé - Echelle - Stochastique - Analyse par ondelettes - Diagraphies soniques - Discontinuités- Lithologie.

*Laboratoire de Géophysique, FSTGAT. USTHB BP32 USTHB, 16111 Bab-Ezzouar, Alger, Algérie
E-mail : nzaourar@usthb.dz
**Laboratoire Dynamique de la lithosphère. UMR5573 UM2/CNRS ; case 060.
Université Montpellier 2, 34095 Montpellier cedex 5 France.
***Géosciences Rennes (CNRS/ INSU UMR 6118), Bât. 15, campus de Beaulieu 35042 Rennes Cedex, France
- *Manuscrit déposé le 14 Janvier 2006, accepté après révision le 07 Mars 2006.*

1 - INTRODUCTION

The sonic logs offer the opportunity to directly access some physical parameters related to the geological characteristics of the medium. These data allow having access to several orders of magnitude in terms of accuracy when compared to surface measurements. Their knowledge in the combination with seismic data, allows the design of reservoir models with an adequate accuracy.

Some preliminary study (Sato, 1984; Kneib, 1995; Holliger, 1996) have shown that the correlation function is used to represent velocity fluctuations. The information from the power spectrum corresponds to the order two statistics and is adequate to describe a Gaussian statistical process with zero mean value. (Holliger, 1996).

Previous research has shown that velocity fluctuations of the sonic logs display scaling behaviour that has been modeled as self affine fractal processes (Wu *et al.*, 1994; Turcotte, 1992, 1997; Holliger, 1996). They are therefore considered as fractional Brownian motion (fBm) (Turcotte, 1992; Holliger, 1996; Li, 1998) and are governed by laws of scale (Mandelbrot, 1983; Flandrin, 1992). Thus, characterizing the scaling behaviour leads to estimating some power law exponents.

The most common method applied to estimate the spectral exponent is based on the Fourier power spectrum. The power spectrum of the velocity log obtained from the Fourier Transform (FT) represents the energy at each wavenumber and therefore shows the importance of each heterogeneity scale, in modelling the regional geological characteristics (Turcotte, 1992). However, this spectrum is not adapted to locate spatial heterogeneity.

The emergence of the wavelet transform analysis in the early eighties is becoming a common tool for analysing local variations of power within the data set. A complete description of geophysical application can be found in Kumar and Foufoula-Georgion (1997).

Many authors have used multiscale wavelet analysis to characterise the singularity order (Holschneïder, 1995; Mallat, 1997; Herrmann, 1997, 1998). Their results have shown that local scale exponents can be estimated from the localized decay/growth rate of wavelet coefficients. However, as discussed by Herrmann (1998), these multiscale methods can not be applied in cases where, either the scale/bandwidth content of the data are too limited or where, the data contains too many interfering transitions. Unfortunately, both situations are typical for well data. However, Herrmann *et al.*,(2001) have introduced a monoscale analysis to measure the sharpness to facies characterisation.

In this paper, we consider extensions of existing results of the stochastic analysis of well data. Both the global spectral exponent estimated by FT and the local spectral exponent obtained from the CWT are discussed. By taking advantage of the central properties of the self affine process, we derive a scaling relation between the wavelet coefficients at different scales from which the scale exponent can be extracted. We have attempted to relate the local variations in the power law exponents from the geological models (synthetics and actual) with geological discontinuities which emerge at small scales. Finally, we conclude with the perspective that the local spectral exponent can be used to distinguish different lithofacies within a formation.

2 - SCALING PROCESS

A scaling process can be characterised by scale laws where the power spectra are approximately inversely proportional to the wavenumber (Mandelbrot, 1983):

$$S(k) \sim k^{-\beta} \qquad (1)$$

The scaling parameter β determines the magnitude of the short and the long term correlations.

Following Pilkington and Todoeschuck (1990, 1991) three special cases may be defined. For the case, $\beta = 0$, its gives a white noise process, when $\beta = 1$, this results to a Joseph noise (Todoeschuck and Jensen 1988), while for the case $\beta = 2$, defines a Brownian noise. Moreover, Holliger, (1996); Turcotte, (1997), have shown a self affinity in geological processes in the sense that if z axis is the depth and s axis indicates one parameter such as the velocity log (i.e. fBm), the scale invariance is given by: $s_{z_0}(\lambda z) \approx \lambda^{H(z_0)} s_{z_0}(z)$ in law where $\lambda \in R^+$, and $H(z_0)$ is the local scale exponent (Hölder exponent) of s function at z_0 and $s_{z_0}(z) \approx s(z+z_0) - s(z)$. In the next section, we will show that the property of the scale invariance by wavelet analysis is well adapted to study self affine processes.

3 - WAVELET ANALYSIS OF SCALING PROCESSES

The wavelet transform is a particularly well adapted tool for analyzing scaling processes. Let us review briefly some of the important properties of wavelets.

The Continuous Wavelet Transform (CWT) of a function s(z) is given by Grossmann and Morlet, (1984) as:

$$C_s(a,b) = \frac{1}{\sqrt{a}} \int_{-\infty}^{+\infty} S(Z)\overline{\psi_{ab}}(Z)dz \qquad (2)$$

each family test function is derived from a single function $\psi(z)$ defined to be as the analyzing wavelet according to (Torresani, 1995):

$$\psi_{a,b}(z) = \psi\left(\frac{z-b}{a}\right) \qquad (3)$$

where, $a \in R^{+*}$ is the scale parameter and $b \in R$ is the translation (- is for the complex conjugate). To be admissible as a wavelet, the analyzing function $\psi(z)$ must have zero mean and be localised in both the space and wavenumber domains. Moreover, ψ is usually chosen to be orthogonal to polynomials. In order to detect a singular behaviour (Hölschneider, 1995), ψ must satisfy the following equation:

$$\int_{-\infty}^{+\infty} z^n \psi(z)dz = 0 \quad \text{for} \quad 0 \le n \le p-1 \qquad (4)$$

According to equation (4), the p moment order of the wavelet coefficients at scale a reproduce the scaling properties of the processes. This scale invariance can be reflected by the CWT as long as the analysing wavelet decreases quickly enough to infinity (Hölschneider, 1995):

$$C_s(\lambda a, z_0 + \lambda b) \approx \lambda^{H(z_0)+\frac{1}{2}} C_f(a, z_0 + b) \qquad (5)$$

This important result shows the property of scale invariance in wavelet analysis to the study of fractal signals. On the other hand, the number of vanishing moments given by relation (4) is directly linked to the regularity of the wavelet transform. More precisely, Hölschneider, (1995); Mallat (1997) showed that a high regularity of the signal is translated via the CWT from the power law variation:

$|C_s(a,b)| \approx a^{H(z_0)+\frac{1}{2}}$ when $a \to 0^+$. Thus, the local power spectrum can be expressed by:

$$|C_s(a,b)| \approx a^{H(z_0)+\frac{1}{2}} \qquad (6)$$

If the analyzing wavelet has enough vanishing moments, the wavelet spectrum exhibits at small scales the same slope as the Fourier spectrum (Perrier *et al.*, 1995).

4 - ESTIMATION OF SPECTRAL EXPONENTS FROM POWER SPECTRUM

The basis of this analysis is a decomposition of the velocity-depth function $V(z)$ in sonic logs into a determinist component $V_d(z)$ and a stochastic component $s(z)$ (Shiomi *et al*, 1997) : $V(z) = V_d(z)(1 + s(z))$

The determinist part $V_d(z)$, generally considered as linear, is suppressed by linear regression. The $s(z)$ stochastic part, also called fractional fluctuations, is modelled by the Von Karman self-correlation function (SCF). The latter characterises a family of self-affine stochastic processes at scales smaller than the correlation length (Goff and Jordan, 1988). These fractional fluctuations can be interpreted as the behaviour of a power law, which comes typically from random fractal phenomena as we have already pointed out in the introduction. In this case, the global power spectrum or Fourier spectrum is given by:

$$p_0(k) \approx k^{-\beta_0} \tag{7}$$

where

$$\beta_0 = 2H + 1 \tag{8}$$

is called the global spectral exponent, H being the number of Hurst and is comprised between 0 and 1.

The local power spectrum is computed via the CWT. In order to build admissible wavelets with first moments p, we use the Gaussian function that is characterized by an infinite number of cancellations able to detect any algebraically behaviours (Perrier *et al*, 1995). In the present study we are interested in the detection of transitions stochastic signals. For this purpose, the Morlet wavelet is particularly adapted to the detection of discontinuities. Its expression is given by:

$\psi(z) = \frac{1}{\sqrt{\pi}} e^{-z^2} e^{-2i\sqrt{\alpha}z}$ where α is the shape parameter of the wavelet and z, the depth.

The algorithm used for the calculation of the CWT is based on the Technique of Multiple Filtering (Li, 1998). In the following, let: $b = z$, the translation given for each depth point z, and the wavenumber k linked to the scale parameter a (Li, 1998) as follows: $k = 2\sqrt{\alpha}/a$

According the equations (6), the local power spectrum or scalogram is then given by:

$$P(k,z) = |C_s(k,z)|^2 \tag{9}$$

For large wavenumbers, this relation can be re-written as: $P(k,z) \approx k^{-\beta(z)}$, where

$$\beta(z) = 2H(z) + 1, \tag{10}$$

describes the local changes of the power law, and is called the local spectral exponent, which is related to the Hölder exponent and to the fractal exponent (Mandelbrot, 1983). For a given wavenumber k, the average of all the wavelet coefficients of $P(k,z)$ spectrum over the total depth z, determines an average wavelet power spectrum $P(k)$ given by the following formula:

$$P(k) = \frac{1}{Z}\int_0^Z P(k,z)dz \tag{11}$$

which can be related to the global power spectrum $P_0(k)$ using the CWT energy conservation. As already stated, both spectra will exhibit at large wavenumbers the same slope since the condition of cancellation of analysing wavelet $\psi(z)$ is verified following the equation (4). In this case, the average wavelet power spectrum can be expressed by the power law:

$$P(k) \approx k^{-\beta_a} \tag{12}$$

where β_a is called the average spectral exponent. To compare both wavelet and Fourier power exponents, we use the following procedure: (1) Calculate the wavelet power spectrum p(k, z) according to equation (9). (2) Compute the average wavelet spectrum p(k) (relation 11). -

(3) Compare average power exponent with the global exponent, using least squares fitting of the power spectra in a log- log plots. (4) In order to locally characterize the heterogeneities, we compute the local spectral exponent over the total depth z of the signal.

5 - APPLICATION

5 - 1 Synthetic models

We start by performing a detailed analysis on a set of generated fBm processes of synthetic logs with predefined Hurst exponents. The quality of a given analyzing method is assessed by the difference between the spectral exponent, more precisely the chosen Hurst number H of the model and the estimated value from the analysis.

The synthetic stochastic fluctuations simulating well data are modelled by filtering a normally distributed random number sequence by the square root of the power spectrum of the Von Karman self-correlation function (Holliger, 1996) in the wavenumber domain.

First, we have tested our approach on synthetic geological models characterised by one, two, three and four layers with different statistical parameters (τ, H and σ). The obtained results indicated that the spectral exponent value is influenced only by the number of Hurst H. For the purpose of extending the efficiency of the method and to assess its resolving power, we suggest four geological models made of several layers which are distinct by the number of samples, Nsamp and, by H value. The standard deviation σ and the correlation length τ were chosen arbitrarily, but the sampling interval is 0.1524m, corresponding to the value of the actual log data.

The velocity fluctuations *s(z)* of the synthetic sonic log (fig. 1) are constructed by putting side by side the fBm eight measurements having distinctive parameters as mentioned in Table I.

Table I - *fBm* processes with $1< \beta <3$ for different layers $C_i (i=1...8)$, where $\beta = 2H+1$, $\sigma = 6\%$, $\tau=25$m.

Processus fBm avec $1< \beta <3$ pour différentes couches $C_i (i=1...8)$, où $\beta = 2H+1$, $\sigma = 6\%$, $\tau=25m$

Layers	C1	C2	C3	C4	C5	C6	C7	C8
Nsamp	512	32	512	32	128	64	256	512
Depth (m)	77.87	82.75	160.78	165.66	185.17	194.92	233.93	311.96
H	0	0.2	0.3	0.5	0.65	0.8	0.95	1
β	1	1.4	1.6	2	2.3	2.6	2.9	3

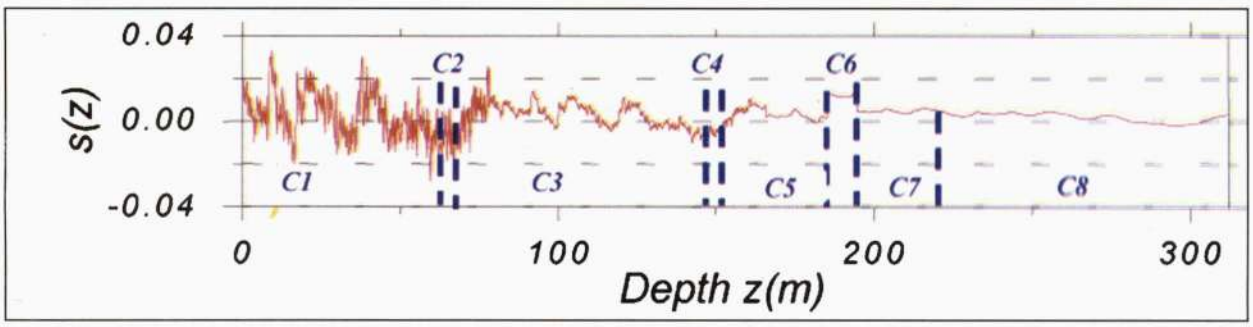

Fig. 1 - The synthetic sonic log velocity fluctuations s(z) for the synthetic geological model. The eight layers differ by their respective values of samples and their rugosity coefficient H.

Fluctuations de vitesse s(z) d'un log sonique synthétique simulant un modèle géologique. Les huit couches (C1, C2, ..., C8) diffèrent par leur nombre d'échantillons et par leur coefficient de rugosité H.

The scalogram (fig. 2) shows the energy distribution. We note that the maximum energy value is in the vicinity of the logarithm of the wavenumber k, being equal to -2.6. This result is confirmed by the four local spectra $P(k, z)$ (fig. 3a1-a4). The spectral exponent values of the local spectra for model 1, taken at various depths z, are given in Table II below:

Indeed, from $log\ k \approx -2.6$, (fig. 3), it can be shown clearly that the local spectra follow the decreasing power law, as described in the previous section. Moreover, in order to have the mean value of the local exponent close to the theoretical value while reducing the uncertainty of the measurements as shown below, several tests performed on the this parameter give the value of α equal to 40 (fig. 3e1, e2). Using the least squares fitting of the power spectra in a log-log plot (fig. 4a, b), it can be noted that the value of the exponent of the average spectral wavelet $\beta = 1.12 \pm 0.06$ is very close to the global exponent $\beta_0 = 1.17 \pm 0.02$ obtained with Fourier spectrum. This result was expected and is linked to the high number of vanishing moments of the Morlet wavelet. Its Fourier transform is given by: $\hat{\psi}(k) = e^{-\frac{1}{4}\left(k+2\sqrt{\alpha}\right)^2}$, hence $\hat{\psi}(0) = e^{-\alpha} \approx 0$ for α=40.

Table II - Comparison between estimated local exponent $\beta(z)$ and predefined exponent.

Comparaison entre l'exposant local $\beta(z)$ estimé et l'exposant prédefini.

Depth z (m)	76	185.2	199.8	233.9
$\beta(z)$	0.89 ± 0.10	1.96 ± 0.18	2.292 ± 0.10	2.26 ± 0.20
β	1	2.3	2.9	2.9

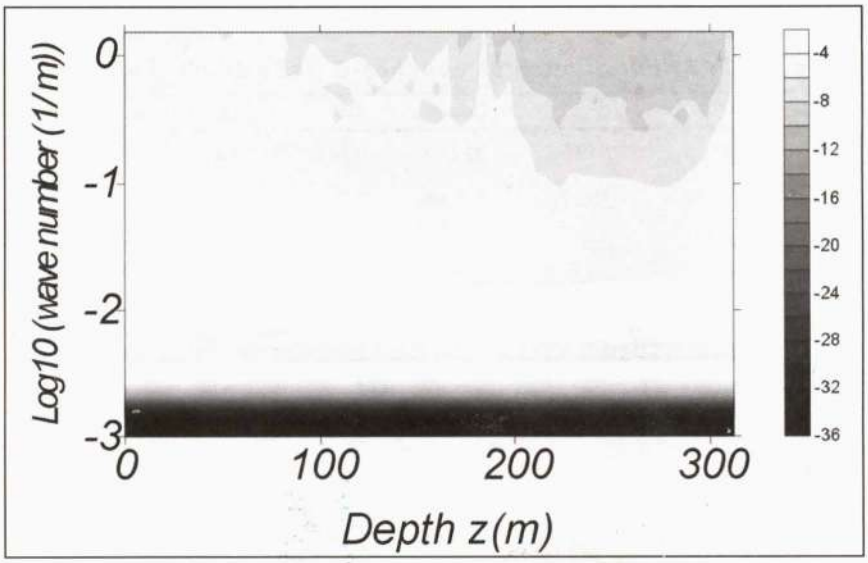

Fig. 2 - Scalogram illustrating the local wavelet power spectrum P(k, z) of signal s(z) in (Fig. 1) using the Morlet wavelet. The energy is coded from white, the minimum, to black, the maximum. The maximum energy value can be noted as being in the vicinity of the logarithm of the wavenumber k = -2.6. The right hand panels shows the scale

Scalogramme représentant le spectre de puissance local par ondelettes P(k, z) du signal s(z) en (Fig. 1), l'énergie est codée du blanc (minimum) au noir (maximum). L'ondelette analysante est l'ondelette de Morlet. Notons que la valeur maximale de l'énergie est au voisinage du logarithme en nombre d'onde k = -2.6. Le schéma à droite indique l'échelle.

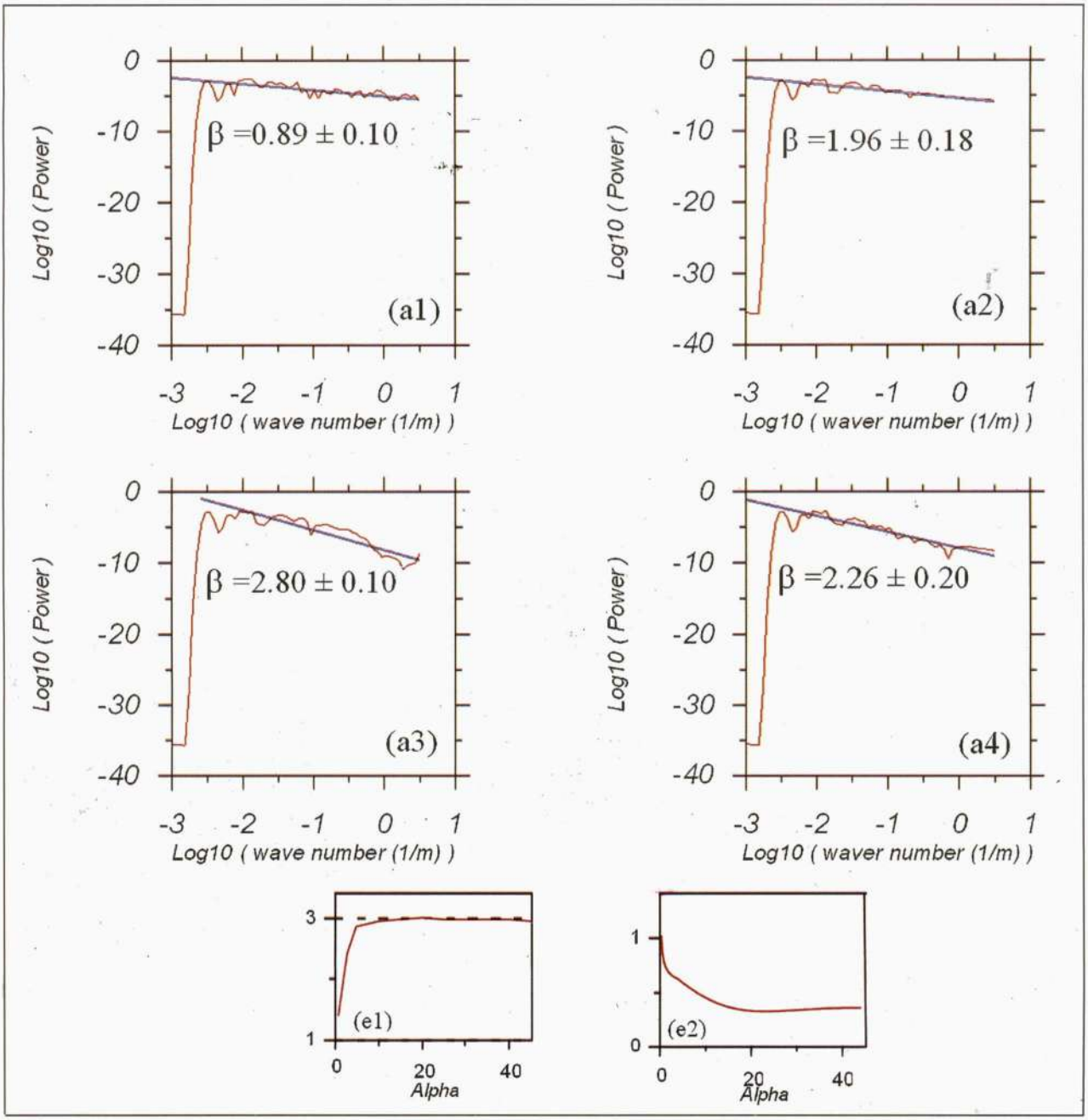

Fig. 3 - Local spectra resulting of 4 cross-sections of the scalogram at depths of 76 m (a1), 185.2 m (a2), 199.8 m (a3) and 233.9 m (a4) respectively, and their corresponding β(z) values. These values can be compared to those of the model in Table II. The straight lines are the least square fitting for the power spectra. The slope given of the regression line is shown at left hand below the spectrum side. (e1) Exponent mean value, (e2) value of uncertainty.

Spectres de puissance locaux obtenus par des coupes du scalogramme aux 4 profondeurs : 76 m (a1), 185.2 m (a2), 199.8 m (a3) et 233.9 m (a4) et les valeurs de β(z) correspondantes. Ces valeurs sont à comparer avec celles du modèle 1(tableau II). Les droites de régression en trait plein sont calculées par ajustement au sens des moindres carrés des spectres de puissance. La pente de ces droites est indiquée du côté gauche sous les spectres. (e1) Valeur moyenne de l'exposant, (e2) valeur de l'incertitude.

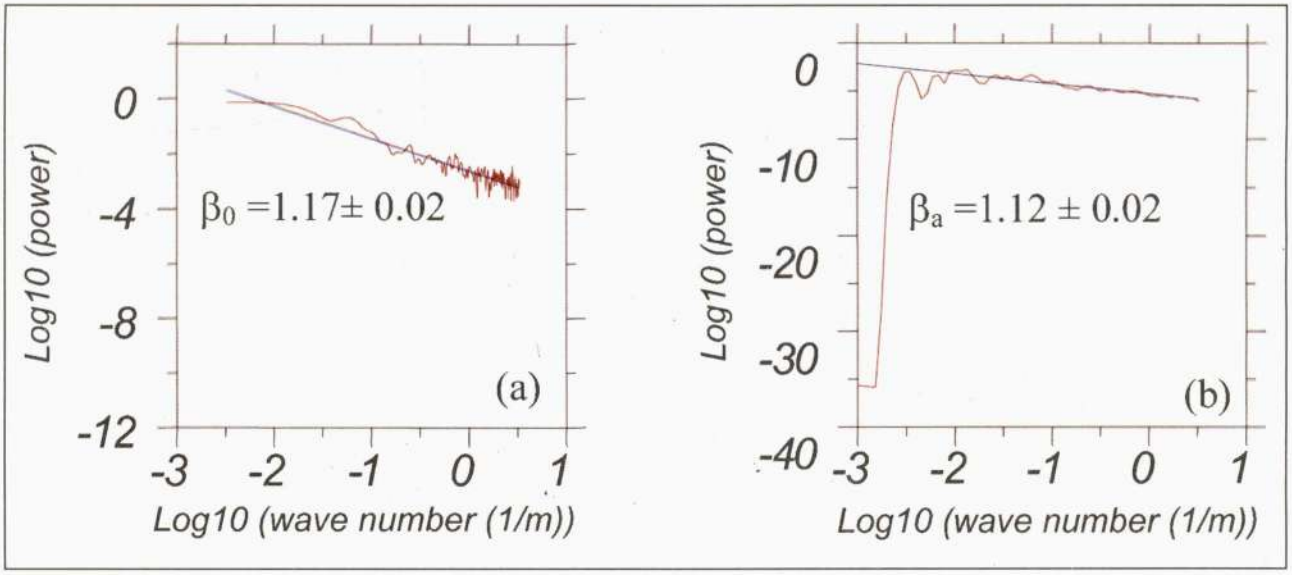

Fig. 4 - (a) Global power spectrum $P_0(k)$ ***(Spectre de puissance global $P_0(k)$)***.
(b) CWT average power spectrum p(k). The straight lines are the least square fitting for the power spectra The comparison between the two spectra slopes indicates very close values ***(Spectre de puissance d'ondelettes moyen p(k). Les droites de régression en trait plein sont calculées par ajustement au sens des moindres carrés des spectres de puissance. La comparaison entre les pentes des droites de régression, montre des valeurs très proches)***.

accordingly, we compute the successive derivatives of $\hat{\psi}(k)$ so as to assess the moments of various orders. We will therefore obtain:

$$\hat{\psi}'(0) = -\sqrt{\alpha}e^{-\alpha} \approx 0\,;\ \hat{\psi}''(0) = -\frac{1}{2}(1-2\alpha)e^{-\alpha} \approx 0\,;$$

$$\hat{\psi}^{(3)}(0) = \left(\frac{3}{2}-\alpha\right)\sqrt{\alpha}\,e^{-\alpha} \approx 0$$

One can note that the moments of order *0*, *1*, *2* and *3* are numerically zero. The zero value is reached because of the exponential term, which decreases very rapidly. We can point out that this result is also valid for moments of very high orders in respect to the value of α. Indeed, we confirm that the average wavelet spectrum shows the same slope as the global spectrum, described by a power law with β as spectral exponent. Local changes of the spectral exponent (fig. 5) show the following situations:

- layers C1 (β=*1.*and *Nsamp. =512*) and C3 (β=*1.6* and *Nsamp. =512*) are retrieved without any ambiguity because of the sufficiently high number of samples.

- Layer C2 (β=*1.4* and *Nsamp. =32*) is thin enough to be not represented.

- Layer C4 (β=*2.*and *Nsamp. =32*) is easily recognisable with a small characteristic peak, despite its thinness.

- The limits of layer C5 (β=*2.3 and Nsamp. =128)* are marked by high amplitude changes in the spectral exponent. The same case is obtained for C6 (β=*2.6* and *Nsamp. =64*), C7 (β=*2.9* and N*samp. =256*) and C8 (β=*3.* and *Nsamp. =512*).

The second model is constructed using the parameters given in the table III.

From the fluctuations *s(z)* and the evolution of the depth spectral exponent (fig. 6), we note the following:

- layers C1 (β=*1.4* and *Nsamp.=512*), C3 (β=*1.6* and *Nsamp.=512*) , C5 (β=*1.8* and *Nsamp.=512*), C7 (β=*2* and *Nsamp.=256*), C9 (β=*3* and *Nsamp. =128*) are clearly reproduced in the plot.

- Layer C2 ($\beta=1.$ and *Nsamp. =16)* is described by a small fairly detected.

- Layers C4 ($\beta=1.2$ and *Nsamp. =32)*, C6 ($\beta=1.4$ and *Nsamp. =64)* are indicated by small steps the width of which depend on the number of the samples of each layer.

- Layer C8 ($\beta=2.5$ and *Nsamp. =16) is* represented by a peak value, different from the theoretical value of the exponent *(2.5)*.

Let us now consider the third model (Table IV) which differs from the second model only by the Hurst value number:

Table III - *fBm* processes with $1<\beta<3$ for different layers C_i *(i=1...9)*, where $\beta = 2H+1$, $\sigma = 6\%$, $\tau=25$m.

Processus fBm avec $1<\beta<3$ pour différentes couches C_i (i=1...9), où $\beta = 2H+1$, $\sigma = 6\%$, $\tau=25m$

Layers	C1	C2	C3	C4	C5	C6	C7	C8	C9
Nsamp	512	16	512	32	512	64	256	16	128
Depth (m)	77.87	80.31	158.34	163.22	241.25	251.01	290.02	292.46	311.96
H	0.2	0	0.3	0.1	0.4	0.2	0.5	0.75	1
β	1.4	1	1.6	1.2	1.8	1.4	2	2.5	3

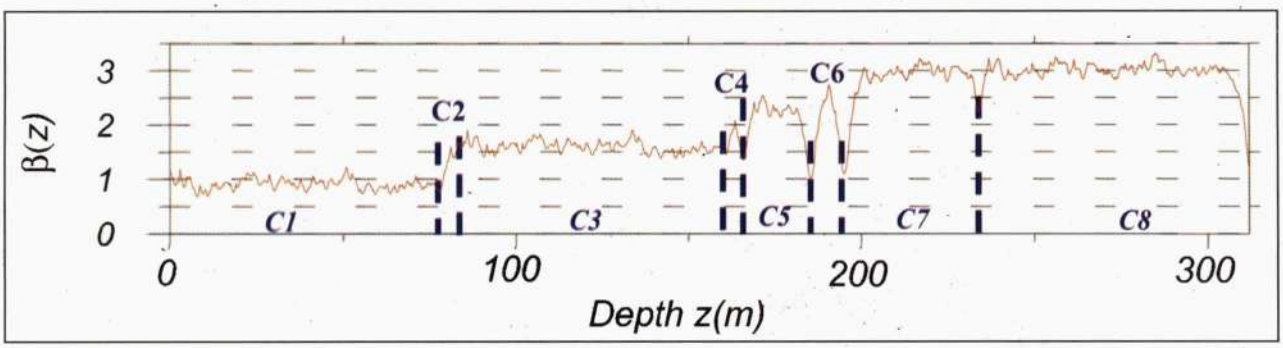

Fig. 5 - Local changes of the spectral exponent $\beta(z)$. The exponent variations show that some discontinuities clearly indicate the layers of model 1 of Fig. 1 .

Changements locaux de l'exposant spectral $\beta(z)$. Les variations de l'exposant montrent que certaines discontinuités reflètent immédiatement les limites des couches du modèle 1(Fig.1)

Table IV - *fBm* processes with $1<\beta<3$ for different layers C_i *(i=1...9)*, where $\beta = 2H+1$, $\sigma = 6\%$, $\tau=25$m.

Processus fBm avec $1<\beta<3$ pour différentes couches C_i (i=1...9), où $\beta = 2H+1$, $\sigma = 6\%$, $\tau=25m$

Layers	C1	C2	C3	C4	C5	C6	C7	C8	C9
Nsamp	512	16	512	32	512	64	256	16	128
Depth (m)	77.87	80.31	158.34	163.22	241.25	251.01	290.02	292.46	311.96
H	0.4	0	0.4	0.1	0.3	0.1	0.4	0	0.3
β	1.8	1	1.8	1.2	1.6	1.2	1.8	1	1.6

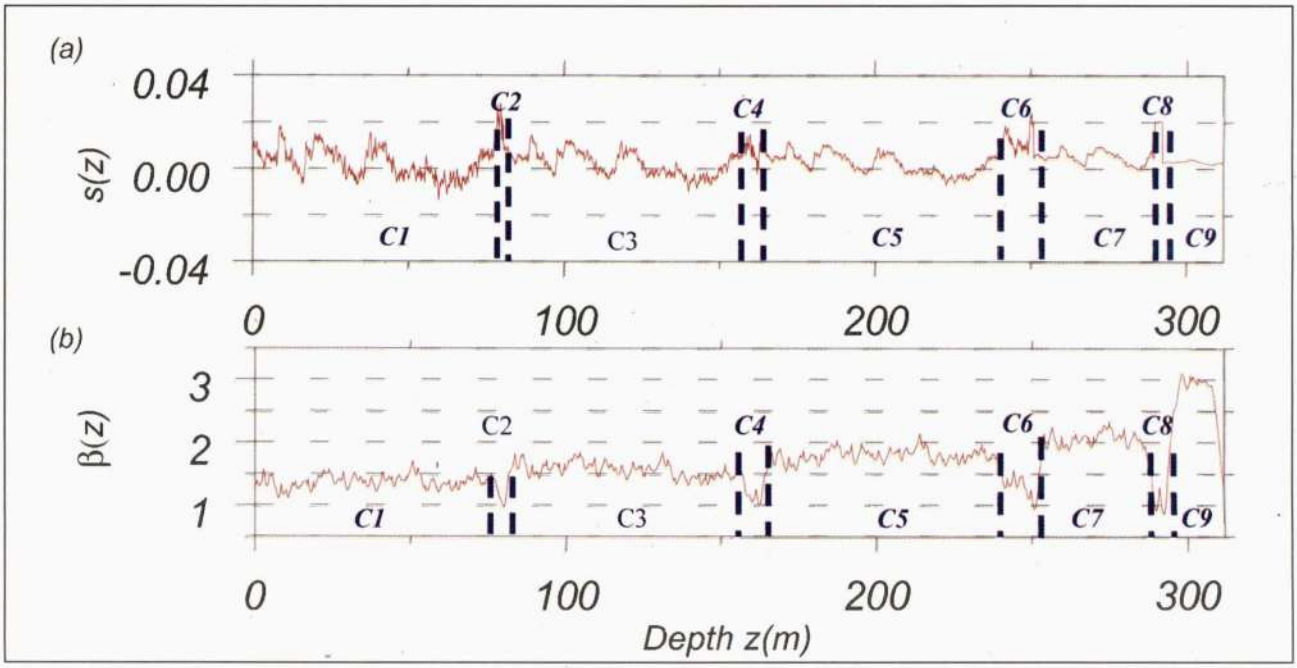

Fig. 6 - Comparison between ***(Comparaison entre)*** : **(a)** the synthetic signal s(z) simulating the velocity fluctuations of the sonic log due to nine layers (C1, C2, C3,.....C9) ***(le signal synthétique s(z) simulant les fluctuations de vitesse d'un log sonique issues des neuf couches (C1, C2, C3,.....C9))*** and, **(b)** the local changes of the spectral exponent β(z). The exponent values show some discontinuities indicating the layers of model 2 ***(les changement locaux de l'exposant spectral β(z). Les variations de l'exposant montrent que certaines discontinuités reflètent immédiatement les limites des couches du modèle 2)***.

By analysing the variation of the spectral exponent over a certain depth interval (fig. 7), one can notice the following:

- Layers C1 ($\beta=1.6$ and $Nsamp.=512$), C3($\beta=1.6$ and $Nsamp.=512$), C5 ($\beta=1.6$ and $Nsamp.=512$), C7 ($\beta=1.8$ and $Nsamp.=256$), C9 ($\beta=1.6$ and $Nsamp.=128$) are faithfully identified in the plot.

- Layers C4 ($\beta=1.2$ and $Nsamp.=32$) and C6 ($\beta=1.2$ and $Nsamp.=64$) are less clearly identified than the previous ones.

- Layers C2 ($\beta=1.$and $Nsamp.=16$) and C8 ($\beta=1.$and $Nsamp.=16$) are represented by a peak; because of the low sample number.

The last model (Table V) is now considered to analyse the influence of the correlation length τ.

This model (fig.8) shows practically similar results to those of model 3 excepting for some differences:

- The exponent values on the layers level C3 and C7 for the model 4 are slightly higher than those the model 3.

- β values corresponding to layers C4 and C8 to model 4 are lower than those of model 3.

This leads us to confirm the non-influence of the τ and σ parameters on the spectral exponent estimation.

We summarise, the results of the computation performed on the four studied models in the table VI given below.

Table V - *fBm* processes with $1< \beta <3$ for different layers C_i $(i=1...9)$, where $\beta = 2H+1$, $\sigma = 6\%$.

Processus fBm avec $1< \beta <3$ pour différentes couches C_i $(i=1...9)$, où $\beta = 2H+1$, $\sigma = 6\%$, $\tau=25m$

Layers	C1	C2	C3	C4	C5	C6	C7	C8	C9
Nsamp	512	16	512	32	512	64	256	16	128
Depth (m)	77.87	80.31	158.34	163.22	241.25	251.01	290.02	292.46	311.96
H	0.4	0	0.4	0.1	0.3	0.1	0.4	0	0.3
β	1.8	1	1.8	1.2	1.6	1.2	1.8	1	1.6
τ *(m)*	25	50	45	10	30	50	60	10	30

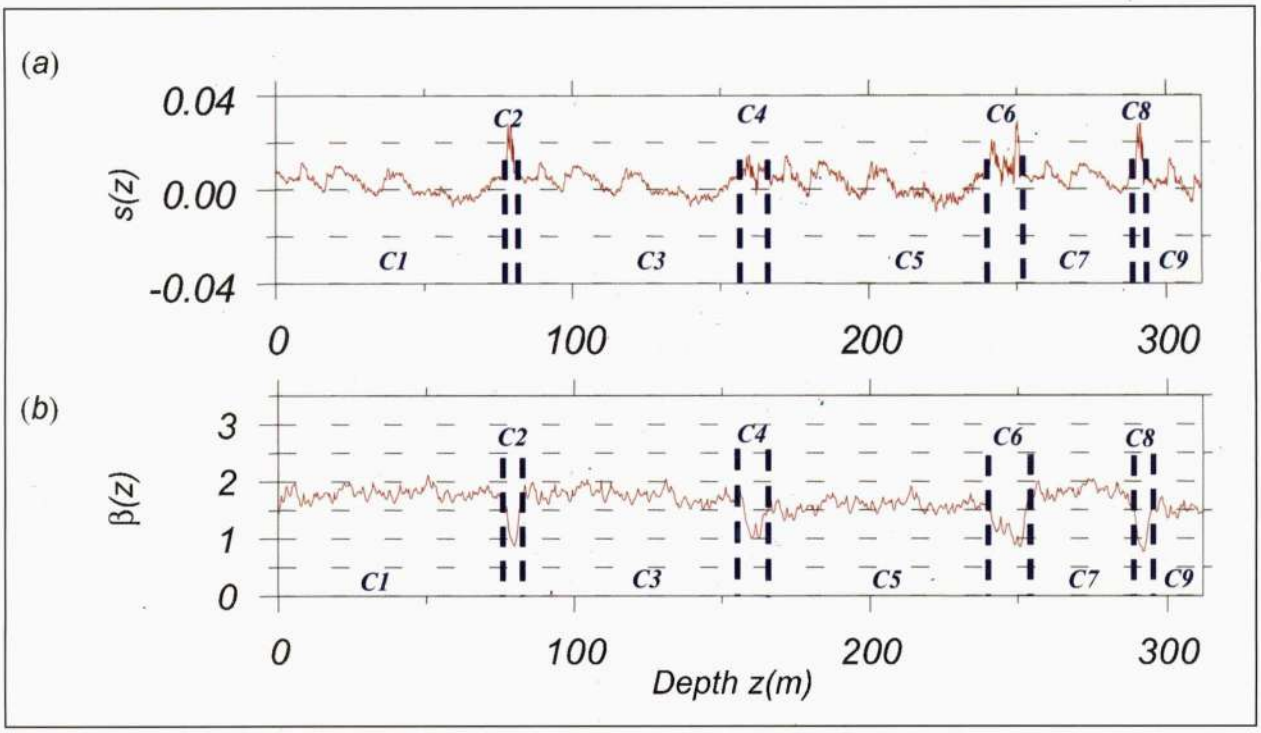

Fig. 7 - Comparison between : (a) the synthetic signal s(z) simulating the velocity fluctuations of the sonic log due to nine layers (C1, C2, C3,.....C9) and, (b) the local changes of the exponent $\beta(z)$. The exponents show some discontinuities indicating the layers of model 3.

Comparaison entre: (a) le signal synthétique s(z) simulant les fluctuations de vitesse d'un log sonique issues des neuf couches (C1, C2, C3,.....C9) et, (b) les changements locaux de l'exposant spectral $\beta(z)$. Les variations de l'exposant montrent que certaines discontinuités reflètent immédiatement les limites des couches du modèle 3.

Table VI - Comparison between the global exponent β_0 and the average exponent β_a.
Comparaison entre l'exposant global β_0 et l'exposant moyen β_a.

Exponents	Model 1	Model 2	Model 3	Model 4
β_0	1.17± 0.02	1.54 ±0.01	1.55 ± 0.01	1.50 ± 0.02
β_a	1.12 ± 0.06	1.51 ± 0.05	1.54 ± 0.05	1.50 ± 0.05
z_0 (m)	76.	304.7	304.7	304.7
$\beta(z_0)$	0.89 ± 0.10	2.97 ± 0.18	1.58 ± 0.11	1.62 ± 0.12

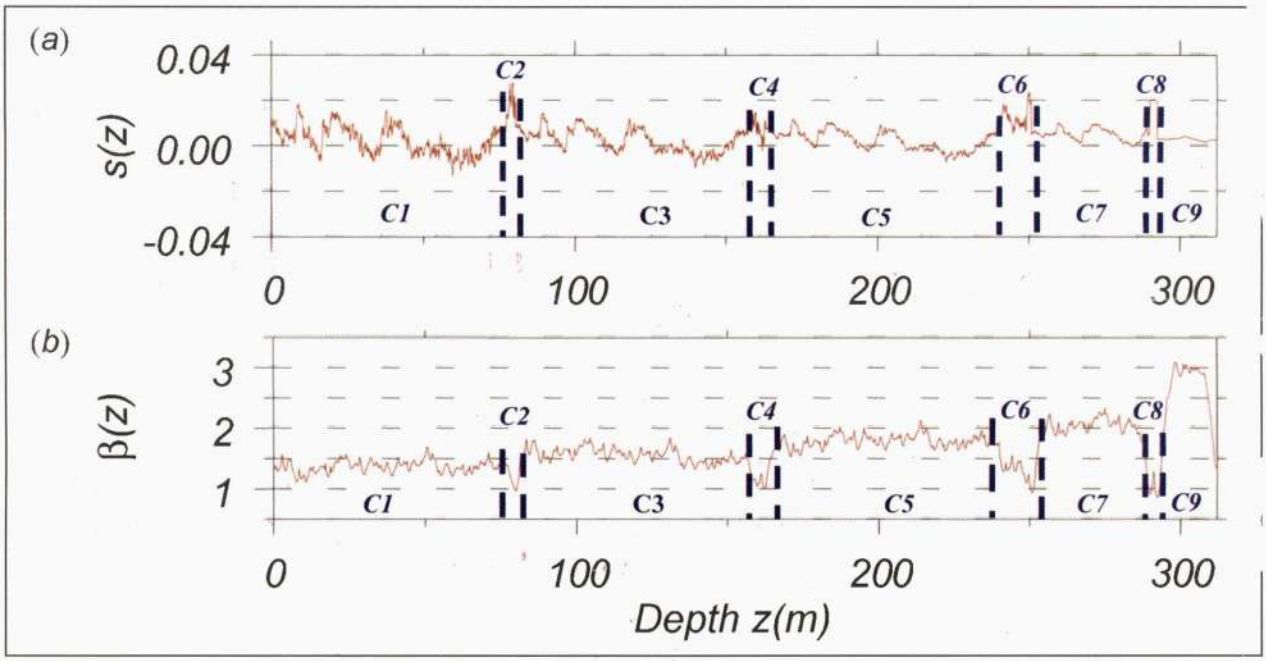

Fig. 8 - Comparison between : (a) the synthetic signal s(z) simulating the velocity fluctuations v(z) of the sonic log due to nine layers (C1, C2, C3,.....C9) and, (b) the local changes of the exponent $\beta(z)$. The exponents show some discontinuities indicating the layers of model 4.

Comparaison entre: (a) le signal synthétique s(z) simulant les fluctuations de vitesse d'un log sonique issues des neuf couches (C1, C2, C3,.....C9) et, (b) les changements locaux de l'exposant spectral $\beta(z)$. Les variations de l'exposant montrent que certaines discontinuités reflètent immédiatement les limites des couches du modèle 4.

On the basis of the above-mentioned results, we can conclude that the method can be efficiently used to separate the various sequences of the studied model. The boundaries of the layers are marked by high changes in the spectral exponent value. We note that the spatial variation of the spectral exponent reflects the various modelled series provided by their thickness (or their sample values) is adequately high. The resolution decreases with the number of samples. The four examples discussed in this section show that the proposed method is able to detect a layer up to *4.72m* thick (*Nsamp.=32*). This is well illustrated by the layer C4 in the models. The latter has a spectral exponent with a difference (in absolute value) of about *0.4* with that of the adjacent layers. In other words, a criterion for detecting a layer can be given by the following:

$$|\beta_{i+1} - \beta_i| \geq 0.4 \quad and \quad |\beta_{i-1} - \beta_i| \geq 0.4$$

We also underline the fact that a *2.29m* layer can be detected if it has a slightly high contrast of the spectral exponent value (of the order of *0.6*).

5 - 2 Application to actual data

To better assess the analysed approach in the detection of discontinuities in the lithologic units, we have extended its application to actual data. Two boreholes in a sedimentary basin situated in the north-east of the Saharan platform have been studied. This basin is considered as a wide Palaeozoic depression in which the crystalline basement is covered with important sedimentary layers and presents a considerable interest in oil exploration.

Table VII below gives the most important statistical parameters of the sonic logs including the average value V_0, standard deviationσ, before and after the linear trend removal, and the constants parameter a and b of the linear regression: $V(z) = b + a\,z$.

Table VII - Statistical parameters of sonic logs

Paramètres statistiques des logs soniques

Wells	V_0 (m/s)	σ_1 (%)	σ_2 (%)	a	b
P1	*4197*	*9.3*	*9.2*	*0.27*	*3355*
P2	4607	18.6	18.5	0.18	4123

The removal of the linear trend causes a decrease in the value of the variance σ. Consequently, in the computation, we have taken into account only the stochastic component *s(z)*.

Well P1

The sonic log (fig. 9) exibits a linear determinist component and the stochastic component of velocity variations *s(z)* for the depth range *2650 – 3550 m*. The signal *s(z)* (fig. 9b) is irregular and exhibits sharp singularities and therefore is suitable for a multiscale analysis based to power law exponent estimation.

The scalogram (fig. 10) illustrates an image with average energy levels ranging from *–0.1 to 1.5*. The maximum energy value is in the vicinity of logarithm wavenumber *k*, equal to *–2.7*. This is confirmed by the sections of the spectrum computed at various depths *z*, and represented by local wavelet spectra (fig.11). The slopes of these straight lines computed in the range *–2.57 to + 0.58, i. e* with spatial wavelengths ranging from *371.5m* to *0.26m*, yield the parameter $\beta(z)$. The spectral exponents (fig.12) obtained by linear regression of the scaling region, are $\beta_a(z) = 1.90 \pm 0.09$ and $\beta_0 = 1.98 \pm 0.01$ for the average power spectrum and Fourier spectrum respectively. One can observe the good agreement between both results. From the variations of the spectral exponent versus depth (fig. 13), we can easily identify the layers C1, C2, C3....to C10. In order to give a geologic meaning to the delineated layers, we describe in Table VIII the lithostratigaphic nature of the considered interval from *2650 to 3550 m*.

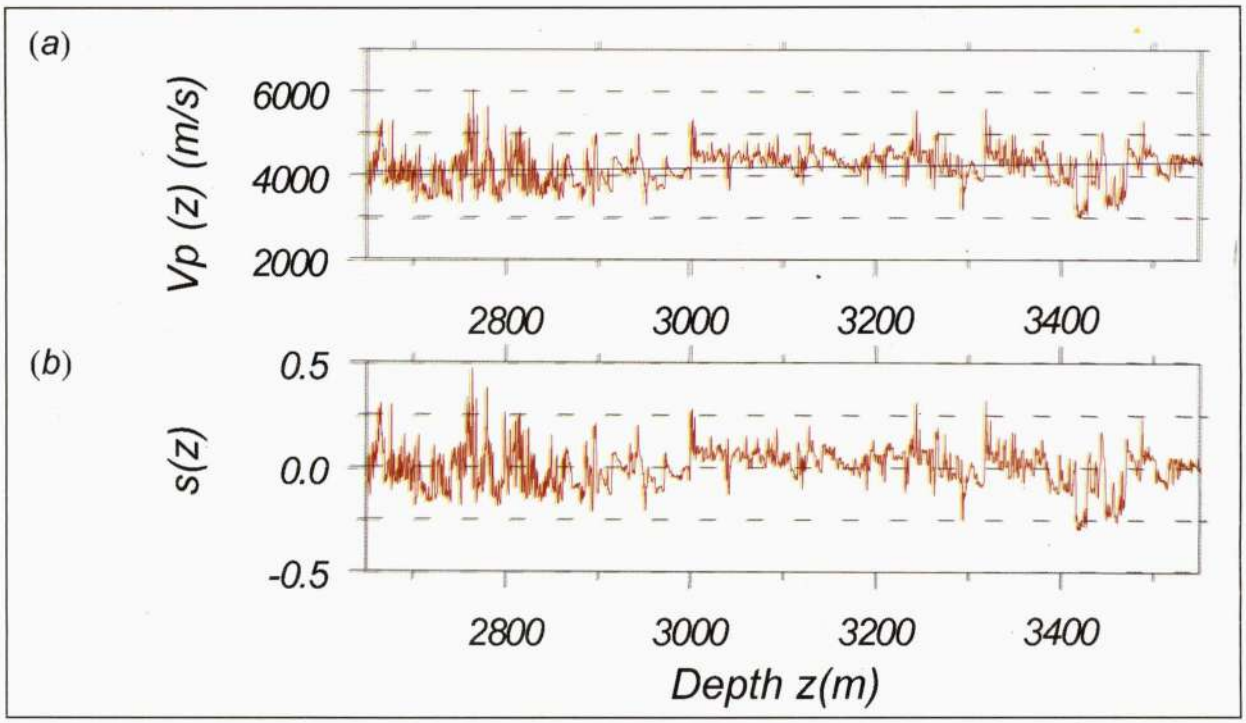

Fig. 9 - **(a)** Plot of the sonic log of the well P1 ***(Trace du log sonique enregistré dans le puits P1)***; **(b)** Distribution of fluctuations s(z) of the corresponding velocity after the linear trend removal ***(Distribution des fluctuations correspondantes de la vitesse s(z) après suppression de la composante déterministe)***.

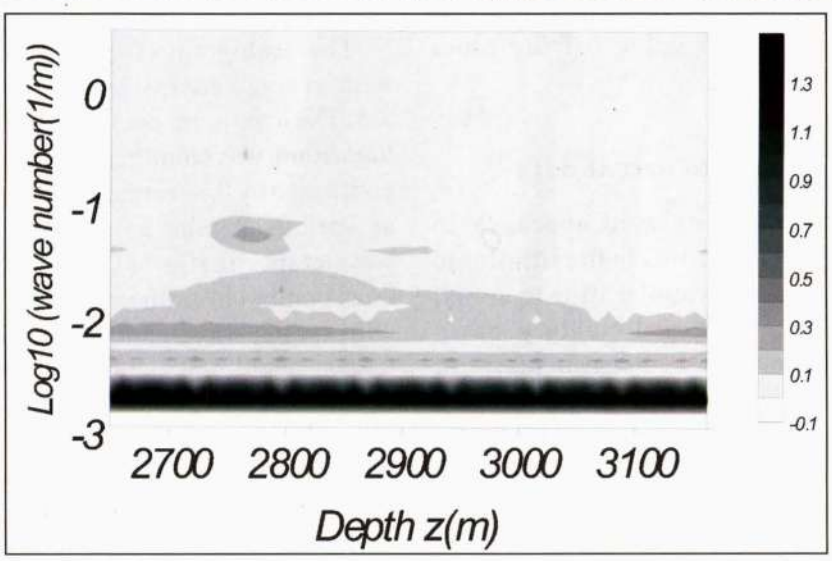

Fig. 10 - Scalogram of the stochastic component s(z) of the sonic log of the well P1 which reflects an image with average energy levels (from – 0.1 to 1.5). The energy is coded from white, the minimum to black, the maximum. The maximum energy value is in the vicinity of the logarithm wavenumber k equal – 2.7. The right hand panels shows the scale.

Scalogramme de la composante stochastique s(z) du log sonique du puits P1 reflétant une image avec des niveaux d'énergie moyens de -0.5 à 1.5. L'énergie est codée du blanc (minimum) au noir (maximum). Notons que la valeur maximale de l'énergie est au voisinage du logarithme en nombre d'onde k = -2.7. Le schéma à droite indique l'échelle.

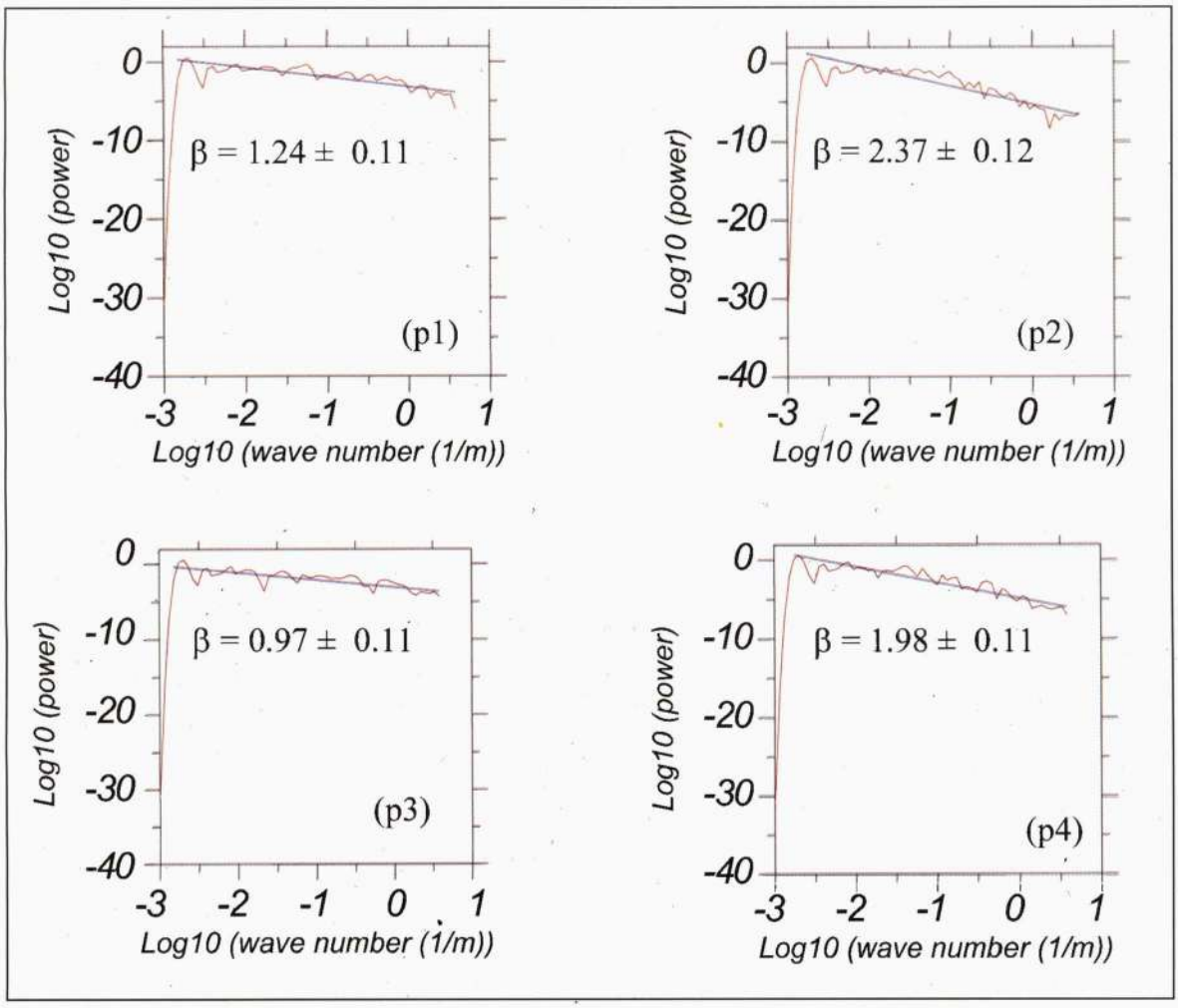

Fig. 11 - Local wavelet spectra resulting of 4 cross-sections of the scalogram at depth of 2775 m (p1), 2873m (p2), 3000 m (p3) and 3150 m (p4) respectively, and their corresponding β(z). The straight lines are the least square fitting for the power spectra in the logarithmic range –2.57 to + 0.58.

Spectres de puissance locaux obtenus par des coupes du scalogramme aux 4 profondeurs : 2775 m (p1), 2873m (p2), 3000 m (p3) et 3150 m (p4) et les valeurs de β(z) correspondantes. Les droites de régression en trait plein sont calculées par ajustement au sens des moindres carrées des spectres de puissance.

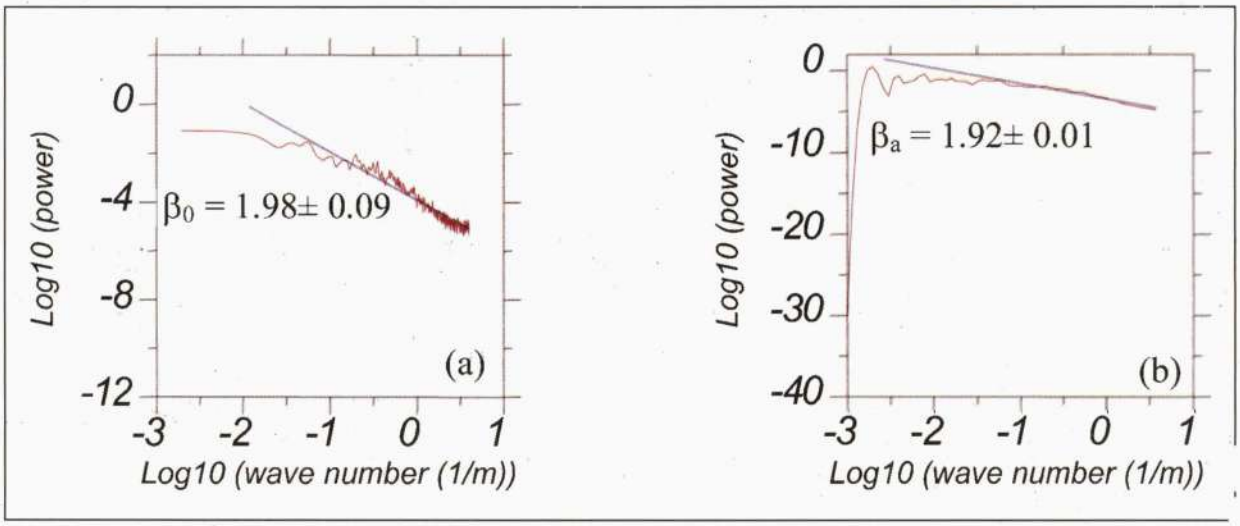

Fig. 12 - **(a)** Global power spectrum $P_0(k)$ ***(Spectre de puissance global $P_0(k)$)***; **(b)** CWT average power spectrum p(k). The straight line are the least square fitting for the power spectra .The slopes tend to be close to the average spectru β_a and the global power spectrum β_0 as illustrated in (a) ***(Spectre de puissance d'ondelettes moyen p(k). Les droites de régression en trait plein sont calculées par ajustement au sens des moindres carrés des spectres d puissance. La comparaison entre les pentes des droites de régression indiquent des valeurs assez proches enti l'exposant spectral moyen β_a représenté en (b) et l'exposant spectral global β_0 représenté en (a))***

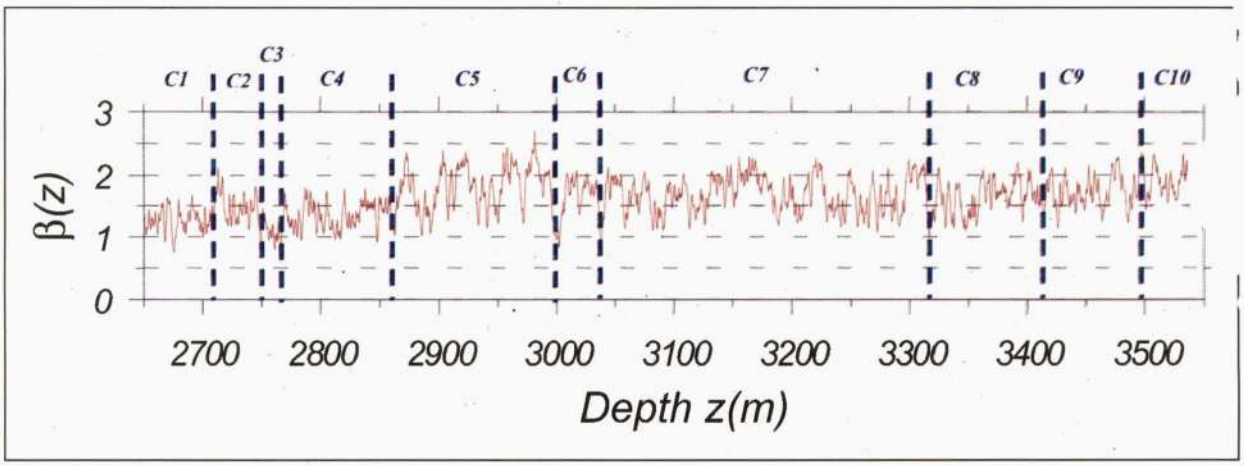

Fig. 13 - **(a)** Plot of the sonic log in the well P2 ***(Trace du log sonique enregistré dans le puits P2)***; **(b)** The fluctuations distribution s(z) of corresponding velocity after the linear trend removal ***(Distribution des fluctuations de vitesse s(z) correspondantes après suppression de la composante déterministe)***.

Table VIII - Correlation between the layers, the lithology and their corresponding average exponents $\beta(z)$ of well P1. (Bekkouche, 1992).

Corrélation entre les couches, la lithologie et leurs exposants moyen $\beta(z)$ correspondants du puit P1. (Bekkouche, 1992).

Facies classification	Layers	Depths (m)	Lithology	$\beta(z)$
A.S.L.T.	*C1*	2660-2710	Predominantly sandstone interbedded with marl layers.	1.3
(2580 –2679)				
	C2	2710-2750	Shale	1.5
	C3	2750-2765	Alternating sandstone and shale.	1.1
Argillaceous	*C4*	2765-2860	Marls with altercation of shale, sandstone and limestone.	1.4
carboniferous				
	C5	2860-3000	Shale interbedded with thin sandstone and silt layers	2.
(2679 – 3188)	*C6*	3000-3040	Shale interbedded with thin sandstone layers.	1.7
	C7	3040-3315	Shale interbedded with thin sandstone and silt layers.	1.8
Upper RKF (3188 – 3408)	*C8*	3315-3415	Marls interbedded with thin sandstone layers.	1.6
Strunian sandstone like (3414- 3528)	*C9*	3415-3500	Sandstone interbedded with thin shale and marl layers	1.7
F2 (3528 – 3981)	*C10*	3500-3550	Alternating Sandstone and Shale	1.8

One can note that the separation of the various layers based on the variation of the spectral exponent is not adequate. This is explained by values rather close to this parameter. A result that we attribute to the prospected geological units presenting a limited lithology (clay and sandstone). Concerning the fluctuations of the exponent value within the same sequence, they are due to interbedded ith thin marl, silt and limestone layers. ccordingly, we considered only the must important changes. We note that the geological formations are characterised by geological layers as described in Table VIII. This can be attributed to the fact that the formations crossed by the well are relatively thick. Also, we obtained that the lithological variations can be related to the average values of their spectral exponents, in the following manner:

- sandstone : 1.3 (C1), 1.7 (C9);
- shale : 1.5 (C2), 1.7 (C6), 1.8 (C7, C10), 2.0 (C5);
- alternating sandstone and shale : 1.1 (C3);
- marl :1.4 (C4), 1.6 (C8).

We can mention that the lithology is not described by one single spectral value but by a set of parameters. A general comparison between the parameter β for different lithologies can therefore suggested :

$$\beta \text{ sandstone} \approx \beta \text{ marl} < \beta \text{ shale}$$

However, the proposed approach cannot detect thin layers, from *5* to *10 m* thick existing in the well. We note that the thinnest layer detected is C3 with is *15m* thick. The latter is probably related to the relative importance of the geological formations of the area.

Well P2

The sonic log and its deterministic and stochastic components are illustrated in (fig. 14). The same computing procedure carried

out for the well P1 allows us to obtain the variation law of the spectral exponent β(z) for the formations of well P2 (fig. 15). The analysis of this figure leads us to identify eleven singularities delineating twelve layers denoted by: C1, C2, C3....C12. The lithostratigraphic formations of the prospected medium from 1950 to 3350 m are described in Table IX.

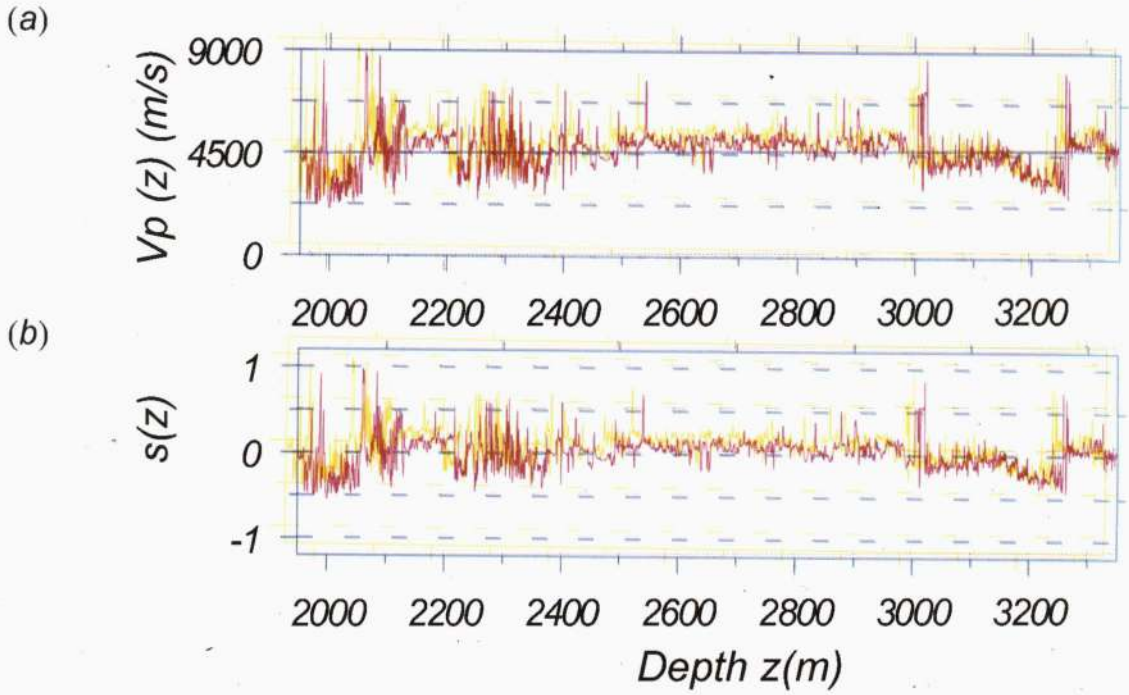

Fig. 14 - Local changes of the spectral exponent β(z). The exponent values show some discontinuities describing the lithology. Indeed, note that the discontinuities delineate the different layers (C1, C2, C3, ...C10).

Changements locaux de l'exposant spectral β(z). Les variations de l'exposant montrent que certaines discontinuités décrivent la lithologie. En effet, notons que ces discontinuités délimitent les différentes couches (C1, C2, C3, ...C10).

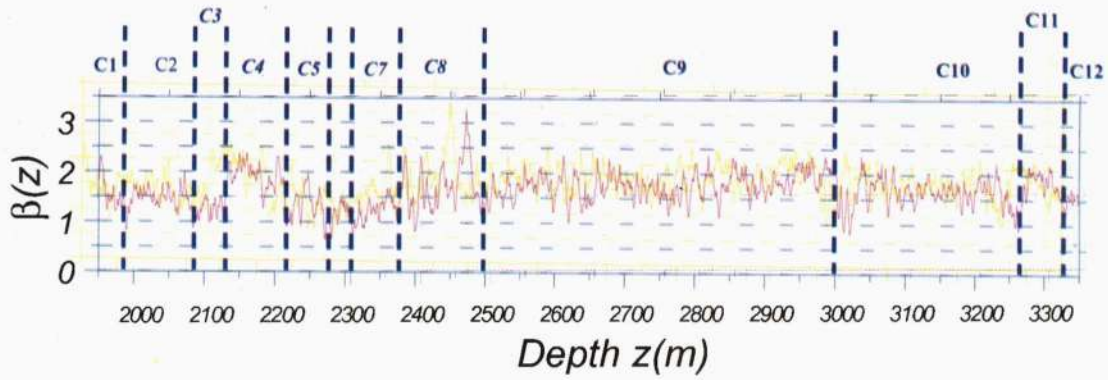

Fig. 15 - Local changes of the spectral exponent β(z). The exponents show some discontinuities describing the lithology. The discontinuities delineate the different layers (C1, C2, C3, ...C12).

Changements locaux de l'exposant spectral β(z). Les variations de l'exposant montrent que certaines discontinuités décrivent la lithologie. En effet, notons que ces discontinuités délimitent les différents couches (C1, C2, C3, ...C12).

Table IX - Correlation between the layers, the lithology and their corresponding average exponents $\beta(z)$ of well P2. (Bekkouche, 1992)

Corrélation entre les couches, la lithologie et leurs exposants moyen $\beta(z)$ correspondants du puit P2. (Bekkouche, 1992).

Facies classification	Layers	Depth (m)	Lithologies	$\beta(z)$
	C1	1960-1990	Dolomitic shale	1.4
Wesphalian- Namurian	*C2*	1990-2085	Dolomitic shale- marl	1.5
(1965 – 2127.5)	*C3*	2085-2127	Argillaceous limestone	1.3
	C4	2127-2215	Argillaceous sandstone	2.
Namurian	*C5*	2215-2280	Shale with sandstone	1.4
(2127.5 – 2292)	*C6*	2280-2310	Shale	1.2
Visean C	*C7*	2310-2375	Argillaceous sandstone	1.3
(2292 – 2638.5)	*C8*	2375-2495	Sandstone interbedded with shale	2.1
Visean B	*C9*	2495-3005	Argillaceous sandstone	1.8
(2638.5 – 2908)				
Tournaisian	*C10*	3005-3260	Shale with sandstone	1.6
(2908 – 3258)				
F2	*C11*	3260-3325	Sandstone interbedded with shale	1.8
(3258 – 3327.5)				
Argillaceous series	*C12*	3325-3350	Argillaceous sandstone	1.6
(3327.5 - 3979)				

We note that the delineation of the various layers for this case is relatively easy compared with the previously studied well. This result can be explained by the clear variations of the spectral exponent. However, we can mention fluctuations in this parameter resulting from the heterogeneous medium. As the wide geological units crossed by the well are thick, each unit is represented by more than a layer. On the basis of the previous table, we try to identify the various lithologies through the average values of their spectral exponents:

- argillaceous limestone: 1.3 (C3);
- shale: 1.2 (C6);
- dolomitic shale: 1.4 (C1), 1.5 (C2);
- shale with sandstone: 1.4 (C5), 1.6 (C10);
- sandstone interbedded with shale: 1.8 (C11), 2.1 (C8);
- argillaceous sandstone: 1.3 (C7), 1.6 (C12), 1.8 (C9), 2. (C4).

The analysis of these results shows that the spectral exponent values that are relative to argillaceous limestone, are similar to those characterising the shale (clean, dolomitic or argillaceous). However, those values are lower than those presented by sandstone:

β argillaceous limestone $\approx \beta$ shale $< \beta$ sandstone

Moreover we note the presence of some thin layers of limestone. To make the analysis of the results easier, we group the slope values of the different spectra related to P1 and P2 wells in Table X.

Table X - Comparison of the global exponent β_0 (FT) with the average exponent β_a (CWT) calculated from sonic logs.

Comparaison entre l'exposant global β_0(FT) et l'exposant moyen β_a(CWT) calculé à partir des logs soniques.

Wells	β_0	β_a	z_0 (m)	$\beta(z_0)$
P1	1.98 ±0.01	1.92 ± 0.09	2774.9	1.24 ± 0.11
P2	1.71 ± 0.01	1.73± 0.09	2200	1.52 ± 0.09

6 - ANALYSIS AND INTERPRETATION OF THE RESULTS

The analysis of these various results of the two wells allows us to make the following comments:

- all the power spectra computed for the stochastic components of the velocity logs have virtually the same shape. They follow power laws of some tens of centimetres to hundreds of meters. The geological media prospected are then self-affine.

- The scalograms practically reflect similar energy distributions with regards to wavenumber-depth (k, z); which we easily checked in their local spectra.

- The good agreement between the global spectral exponent β_0 and average exponent β_a calculated and good quality of regression fit is due to the suitable choose of analysing wavelet and scale range in which the power spectra follow algebraically decreasing law.

- A well-defined geological facies does not have in the same well a single spectral exponent value, but rather values distributed in an interval. Equally, this facies is characterized by non-correlated values when moving from a well to another. To better illustrate that, let us consider for instance the case of clay which have exponent values higher than that which identify sandstone in Well P1. Now as for borehole P2, the reverse takes place: sandstone reflects the highest values. We therefore conclude that spectral exponent β may be considered as a very good lithological index.

The finest layers detected above have a thickness of *15m* for well P1 and *25m* for well P2. We note that the resolving power of the method is not constant. It dependants on the thickness of a layer and of the lithology of the neighbouring layers. More precisely, this resolution is spectral exponent layers dependent.

7 - CONCLUSION

We have shown that spectral exponent estimation based on the CWT can be adapted to characterise velocity fluctuations of sonic log. When suitable scaling proprieties are observed both scalogram and global power spectrum display similar power law. In this case, the power law exponent $\beta(z)$ can be used to distinguish different lithofacies within a formation. The interpretation of the geological interfaces as shown by our results indicates that a well-defined geological facies is not characterised by a specific value of the spectral exponent. We therefore conclude that spectral exponent remains a good lithological index and can be used to prove an existence of lithofacies which cannot be detected from others well logs.

REFERENCES

BEKKOUCHE, D., 1992. Le Silurien Dévonien inférieur du bassin de Ghadamès (Sahara oriental algérien) : Lithostratigraphie, Sédimentologie et Diagenèse des réservoirs gréseux. *Thèse de doctorat, université Joseph Fourier, Grenoble I., 302p.*

FLANDRIN, P., 1992. Wavelet analysis and synthesis of Fractional Brownian Motion. *IEEE transformation on Information Theory*, 38, 910-917.

GOFF, J.A. AND JORDAN, T.H., 1988. Stochastic modelling of sea floor morphology : inversion of sea beam data for second order statistic. *Journal of Geophysical Research*, 93, 13589-13608.

GROSSMANN, A. AND MORLET, J., 1984. Decomposition of hardy functions into square integral wavelets of constant shape, SIAM J. *Math. Anal.*, 15, 723-736.

HERRMANN, F.J., 1997. A scaling medium representation, a discussion of well-logs, fractals and waves. *Thesis, Delft University of Technology, Delft, The Netherlands.*

HERRMANN, F., 1998. Multiscal analysis of well and Seismic data, in *Mathematical Methods in Geophysical Imaging V, edited by S. Hassanzadeh,* vol. 3453, 180-208, SPIE.

HOLLIGER, K., 1996. Upper crustal seismic velocity heterogeneity as derived from a variety of P-wave sonic logs. *Geophysical Journal International* 125, 813-829.

HÖLSCHNEIDER, M., 1995. Wavelets: An Analysis Tool, 423 p., Clarendon, Oxford England.

KNEIB, G., 1995. The Statistical nature of the upper continental crystalline crust derived from in situ seismic measurements. *Geophysical Journal International* 122, 594-616.

KUMAR, P. AND FOUFOULA-GEORGIOU, E., 1997. Wavelet analysis for geophysical applications, *Reviews of geophysics,* 35, 4, 385-412.

LI, X.P., 1998. Wavelet power spectrum analysis of heterogeneities from sonic velocity logs. *Geophysical Prospecting.*, 46, 455-475.

MALLAT, S., 1997. A Wavelet Tour of Signal Processing, 627, *Academic Press.*

MANDELBROT, B.B., 1983. The fractal geometry of nature : W. H. Freeman, *San Francisco.*

PERRIER, V., PHILIPOVITCH, T. AND BASDEVANT, C., 1995. Wavelet spectral compared to Fourier spectra, *J. Math. Phys.*, 36, 1506- 1519.

PILKINGTON M. AND J. P. TUDOESCHUCK 1990. Stochastic inversion for scaling geology. *Geophysical Journal International* 102, 205-217.

PILKINGTON M. AND J. P. TUDOESCHUCK 1991. Naturally smooth inversion with a priori information from well logs. *Geophysics*, 56, N°11, 1811-1818.

SATO, H., 1984. Attenuation and envelope formation of three components of small local earthquakes in randomly inhomogeneous lithosphere. *Journal Geophysical Research* 89, 1221-1241.

SHIOMI K., H. SATO AND M. OHTAKE 1997. Broad-band power-law spectra of well-log data in Japan. *Geophysical Journal International.*, 130, 57-64.

TORRESANI, B., 1995. Analyse continue par ondelettes, 239 p. Inter Editions / *CNRS Edition.*

TODOESCHUCK, J.P. AND JENSEN, O.G., 1988. Josef geology and seismic deconvolution, *Geophysics,* 53, 1410-1414.

TURCOTTE, D.L., 1992. Fractal and chaos in geology geophysics, *Cambridge University. Press, Cambridge,* 337 p.

TURCOTTE, D.L., 1997. Fractal and chaos in Geology and Geophysics, 337 p. *Cambridge University, Press Cambridge.*

WU, R.S., XU, Z. AND LI X. P., 1994. Heterogeneity spectrum and scale anisotropy in the upper crust revealed by the German Continental Deep Drilling (KTB) Holes. *Geophysical Research Letter*, 21, 911-914.